

# The importance of turbulent ocean-sea ice nutrient exchanges for simulation of ice algal biomass and production with CICE6.1 and Icepack 1.2

Pedro Duarte<sup>1</sup>, Philipp Assmy<sup>1</sup>, Karley Campbell<sup>2,3</sup>, Arild Sundfjord<sup>1</sup>

<sup>1</sup> Norwegian Polar Institute, Fram Centre, Tromsø, Norway

<sup>2</sup> Department of Arctic and Marine Biology, UiT The Arctic University of Norway, Norway

<sup>3</sup> Bristol Glaciology Centre, University of Bristol, UK

*Correspondence to:* Pedro Duarte (Pedro.Duarte@npolar.no)

**Abstract.** Different sea-ice models apply unique approaches in the computation of nutrient diffusion between the ocean and the ice bottom, which are generally decoupled from the calculation of turbulent heat flux. Often, a simple molecular diffusion formulation is used. We argue that nutrient transfer from the ocean to sea ice should be as consistent as possible with heat transfer, since all these fluxes respond to varying forcing in a similar fashion. We hypothesize that biogeochemical models which do not consider such turbulent nutrient exchanges between the ocean and the sea-ice, despite considering brine drainage and bulk exchanges through ice freezing/melting, may underestimate bottom-ice algal production. The Los Alamos Sea Ice Model (CICE + Icepack) was used to test this hypothesis by comparing simulations without and with diffusion of nutrients across sea-ice bottom dependent on velocity-shear, implemented in a way that is consistent with turbulent heat exchanges. Simulation results support the hypothesis, showing a significant enhancement of ice algal production and biomass when nutrient limitation was relieved by bottom-ice turbulent exchange. Our results emphasize the potentially critical role of turbulent exchanges to sea ice algal blooms, and the importance of thus properly representing them in biogeochemical models. The relevance of this becomes even more apparent considering ongoing trends in the Arctic Ocean, with a predictable shift from light to nutrient limited growth of ice algae earlier in the spring, as the sea ice becomes more fractured and thinner with a larger fraction of young ice with thin snow cover.

## 1 Introduction

Momentum, heat and mass fluxes between the ocean and the sea-ice are of utmost importance to predict sea-ice motion, thermodynamics, and biogeochemistry. However, when we look at models released over the last decades, we find not only inter-model differences in the physical concepts used to describe the processes responsible for some of the above fluxes, but also intra-model differences in the approaches used in calculating, for example, heat and mass fluxes. In this work we will focus on the differences related with the vertical diffusion of tracers between the water column and the bottom-ice and attempt to explore their consequences on nutrient limitation for sea-ice algal growth.

31 We may divide the ocean-ice exchange processes into those related to: (i) entrapment during freezing; (ii) flushing and release  
32 during melting;(iii) brine gravity drainage, driven by density instability, parameterized as either a diffusive or a convective  
33 process; (iv) molecular diffusion; and (v) turbulent diffusion at the interface between the ocean and the ice induced by velocity  
34 shear – the latter process being the focus of this study (e.g. Arrigo et al, 1993 and references therein; Jin et al., 2006; McPhee,  
35 2008; Notz and Worster, 2009; Turner et al., 2013; Tedesco and Vichi, 2010, 2019; Jeffery et al., 2011; Vancoppenolle et al.,  
36 2013).

37 These processes are considered in several sea ice models. Arrigo et al. (1993) distinguished nutrient exchanges resulting from  
38 gravity drainage in brine channels, from brine convection in the skeletal layer, dependent on the ice growth rate. These brine  
39 fluxes were used to calculate nutrient exchanges as a diffusive process. Lavoie et al. (2005) also calculated nutrient exchanges  
40 as a diffusive process. Jin et al. (2006; 2008) computed nutrient fluxes across the bottom layer as an advection process  
41 dependent on ice growth rate and based on Wakatsuchi and Ono (1983). Molecular diffusion was also considered. More  
42 recently, other authors have integrated formulations of “enhanced diffusion” (Vancoppenolle et al., 2010; Jeffery et al., 2011)  
43 or convection (Turner et al., 2013), based on hydrostatic instability of brine density profiles, to compute brine gravity drainage  
44 and tracer exchange within the ice and between the ice and the sea water. Comparisons between salt dynamics in growing sea  
45 ice with salinity measurements showed that convective Rayleigh number-based parameterizations (e.g. Wells et al., 2011),  
46 such as the one by Turner et al. (2013), outperform diffusive and simple convective formulations (Thomas et al., 2020).

47 Interestingly, heat exchange is often calculated differently from salinity in models. In the case of the former, typically, a  
48 transfer mechanism (turbulent or not) at the interface between the ocean and the sea ice is not dependent on any type of brine  
49 exchange. In the case of salinity, such a mechanism is not considered (e.g. Vancoppenolle et al., 2007; Turner et al., 2013).  
50 Presumably, such differences result from the relative importance of various physical processes for different tracers. Heat  
51 transfer between the ice and the water is a fundamental mechanism in explaining sea-ice thermodynamics, irrespective of brine  
52 exchanges. On the other hand, ice desalination depends mostly on brine gravity drainage and flushing during melting (Notz  
53 and Worster, 2009).

54 Vertical convective mixing of nutrients under the sea ice may result from brine rejection and/or drainage from the sea ice (Lake  
55 and Lewis, 1970; Niedrauer and Martin, 1979; Reeburgh, 1984) and from turbulence due to shear instabilities generated by  
56 drag at the interface between the ocean and the sea ice (Gosselin et al., 1985; Cota et al., 1987; Carmack, 1986), internal waves  
57 and topographical features (Ingram et al., 1989; Dalman et al., 2019). Gosselin et al. (1985) and Cota et al. (1987) stressed the  
58 significance of tidally induced mixing in supplying nutrients to sympagic algae. Biological demand for silicic acid (hereafter  
59 abbreviated as silicate) and nitrate is limited by the physical supply (Cota and Horne, 1989; Cota and Sullivan, 1990).

60 The analysis of several models published over the last decades and their approaches to calculate tracer diffusion across the ice-  
61 ocean interface shows that some models do not consider this process or limit it to molecular diffusion. Other models consider  
62 turbulent exchanges parameterized as a function of the Rayleigh number, calculated from brine vertical density gradients. Only  
63 one of the sampled models (Mortenson et al., 2017) uses a parameterization based on friction velocity. In the absence of ice  
64 growth and when brine gravity drainage is limited, diffusive nutrient exchanges between the ocean and the ice have the capacity

65 to limit primary production. This limitation will be alleviated in the presence of a turbulent exchange mechanism. We argue  
 66 that nutrient transfer at the interface between the ocean and the sea ice should be as consistent as possible with heat transfer  
 67 since all these fluxes are closely linked. We hypothesize that models which do not consider the role of current velocity shear  
 68 on turbulent nutrient exchanges between the ocean and the sea-ice may underestimate bottom-ice algal production.  
 69 To test the above hypothesis, we use a 1D vertically resolved model and contrast results using the default diffusion  
 70 parameterization and a “turbulent” parameterization analogous to that of heat transfer, at the interface between the ocean and  
 71 the sea ice, based on McPhee (2008).

## 72 **2 Methods**

### 73 **2.1 Concepts**

74 Turbulent exchanges may be parameterized through the flux of a quantity at the interface between the ocean and the sea ice,  
 75 calculated as the product of a scale velocity and the change in the quantity from the boundary to some reference level (McPhee,  
 76 2008):

$$77 \langle w'S' \rangle = \alpha_s u^* (S_w - S_0) \quad (1)$$

78 Where,  $\langle w'S' \rangle$  represents the averaged co-variance of the turbulent fluctuations of interface vertical velocity ( $\text{m s}^{-1}$ ) and  
 79 salinity, respectively,  $\alpha_s$  is an interface salt/nutrient exchange coefficient (dimensionless);  $u^*$  is the friction velocity ( $\text{m s}^{-1}$ );  $S_0$   
 80 and  $S_w$  are interface and far-field salinities, respectively.

81 Hereafter we will assume that salt turbulent exchanges are similar to nutrient exchanges and governed by the same principles  
 82 and parameters. The main difference between turbulent heat and salt/nutrient exchanges is due to the exchange coefficients  
 83 that may be higher for heat. The heat exchange coefficient ( $\alpha_h$ ) is around 0.006. The ratio ( $R$ ) between  $\alpha_h$  and  $\alpha_s$  may vary from  
 84 unity to a range between 35 and 70 during ice melting and because of double diffusion, leading to a range in  $\alpha_s$  between  $8.6$   
 85  $10^{-5}$  and 0.006 (McPhee et al., 2008).

86 The net downward heat flux from the ice to the ocean in the Los Alamos Sea Ice Model (CICE + Icepack) is given by (Hunke  
 87 et al., 2015) and it is computed according to McPhee et al. (2008) [Eq. (2)]:

$$88 F_{bot} = -\rho_w c_w \alpha_h u^* (T_w - T_f) \quad (2)$$

89 Where,  $\rho_w$  is the density of seawater ( $\text{kg m}^{-3}$ );  $c_w$  is the specific heat of seawater ( $\text{J kg}^{-1} \text{K}^{-1}$ );  $\alpha_h$  is the heat transfer coefficient  
 90 (dimensionless);  $T_w$  is the water temperature (K);  $T_f$  if the freezing temperature (K).

91 We calculate salt or nutrient exchanges using a similar approach:

$$92 F_N = -\alpha_s u^* (N_w - N_0) \quad (3)$$

93 In fact, this is an extension of the concept used for heat and salt by McPhee (2008) (see page 112, Fig. 6.3). The minus sign  
 94 used in (3) and (4) is for compatibility with the CiCE + Icepack convention that upward fluxes are negative (e.g. Hunke et al.,  
 95 2015).

96 A timescale for this turbulent process may be calculated from:

$$97 \quad \tau = \frac{\alpha_s u^*}{z} [s^{-1}] \quad (4)$$

98 Where  $z$  is a vertical distance (m) ( $h$  in the Los Alamos Sea Ice Model, see below). The above time scale is calculated for  
99 consistency with CICE implementation of diffusion, where a comparable time scale is calculated as:

$$100 \quad \tau = \frac{D_m}{h^2} [s^{-1}] \quad (5)$$

101 Or

$$102 \quad \tau = \frac{D_{MLD}}{h^2} [s^{-1}] \quad (6)$$

103 Where  $D_m$  is the molecular diffusion coefficient and  $D_{MLD}$  is the mixed length diffusion coefficient ( $m^2 s^{-1}$ ) (Jeffery et al., 2011).  
104 In the Los Alamos Sea Ice Model,  $h$  corresponds to the thickness of the biogeochemical grid (biogrid). This is the non-  
105 dimensional grid used for discretizing the vertical transport equations of biogeochemical tracers, defined between the brine  
106 height, which takes the value zero, and the ice-ocean interface, which takes the value one (Jeffery et al., 2016). The usage of  
107  $h$  in these timescales implies merely the way they are normalized in the code before the actual diffusive fluxes are calculated  
108 considering the distance between the points ( $h \cdot \partial x$ , see below equation 7) where variables are calculated, along the layers of  
109 the biogrid. The product  $h \cdot x$  corresponds to the actual distance of a given point from the top of the biogrid. The time scales  
110 expressed in equations 5 and 6 are included in the Icepack transport equation, which may be written as [for more details, refer  
111 Jeffery et al. (2011; 2016)]:

$$112 \quad \varphi \frac{\partial N}{\partial t} = \left\{ \frac{(x-1)}{h} \frac{\partial z_t}{\partial t} - \frac{x}{h} \frac{\partial z_b}{\partial t} \right\} \frac{\partial}{\partial x} (\varphi N) + \frac{1}{h} \frac{\partial}{\partial x} (w_f N) + \frac{\partial}{\partial x} \left( \frac{D_{MLD} + \varphi D_m}{h^2} \frac{\partial N}{\partial x} \right) \quad (7)$$

113 Where  $0 \leq x \leq 1$  is the relative depth of the vertical domain of the biogrid,  $z_t$  and  $z_b$  are vertical positions of the ice top and  
114 bottom (m), respectively,  $\varphi$  is sea ice porosity,  $w_f$  is the Darcy velocity due to the sea ice flushing of tracers ( $m s^{-1}$ ).  $D_{MLD}$  is  
115 detailed in Jeffery et al. (2011) and it is zero when the brine vertical density gradient is stable, otherwise (when density  
116 increases towards the ice top) it is calculated as:

$$117 \quad D_{MLD} = \frac{gk}{\mu} \Delta \rho_e l \quad (8)$$

118 Where  $g$  is the acceleration of gravity ( $9.8 m s^{-2}$ ),  $k$  is sea ice permeability,  $\mu$  is dynamic viscosity ( $2.2 kg m^{-1} s^{-1}$ ),  $\rho_e$  is the  
119 equilibrium brine density and  $l$  is a length scale (7 m). The values shown here are the default ones in Icepack.

120 The last term of equation 7 includes the contribution of molecular diffusion that is calculated at the interface of all layers of  
121 the biogrid and at the interface of the last layer and the ocean. In the simulations using turbulent diffusion, we perform the  
122 same calculations, except that the molecular diffusion term  $\frac{\varphi D_m}{h^2}$  is replaced with a turbulent diffusion term  $\frac{\alpha_s u^*}{h}$   
123 between the last model layer and the ocean.

124 The transport equation is resolved along the biogrid, with a Flux-Corrected, Positive Definite Transport Scheme, using the  
125 finite element Galerkin discretization (Jeffery et al., 2016). In the case of the bottom ice layer, tracer concentrations are  
126 calculated at the ice-ocean interface.

127 Therefore, in the CICE model the implementation of turbulent diffusion nutrient exchanges at the ice-ocean interface in terms  
128 consistent with heat exchanges is quite straightforward, depending on changing the timescales from Eq. (5) to (4). In other  
129 models, other approaches may be required.

130 From equations 4 - 6 it turns out that the product  $\alpha_s u$  by distance ( $z$ ) has the same dimensions of  $D_m$  or  $D_{MLD}$ , corresponding to  
131 a turbulent diffusion coefficient. Assuming  $z \approx 0.01$  m, turbulent diffusion induced by velocity shear, becomes comparable with  
132 molecular diffusion only for  $u^* < 0.0012$  m s<sup>-1</sup>, considering the lower end of the  $\alpha_s$  range ( $8.6 \cdot 10^{-5}$ , see above) or  $u^* < 1.7 \cdot 10^{-5}$   
133 m s<sup>-1</sup>, considering the upper end of the  $\alpha_s$  range (0.006). If we assume instead  $z \approx 0.001$  m, the calculated  $u^*$  values increase by  
134 one order of magnitude but are still very low. In fact, such low friction velocities would require extremely low “stream”  
135 velocities - relative ice-ocean velocities. For an account of the relationship between “stream” and friction velocities under the  
136 sea ice see Supplementary information 3 of Olsen et al. (2019) and references therein. These authors show that “stream”  
137 velocities of only a few centimetres per second lead to friction velocities one order of magnitude lower but still in the order of  
138  $0.001$  ms<sup>-1</sup>, i.e., comparable only to the highest  $u^*$  estimated above. Considering current velocities relative to the sea ice  
139 observed during the N-ICE2015 cruise [Granskog et al., 2018; Figure 2d of Duarte et al. (2017)], with most values between  
140  $0.05$  and  $> 0.2$  m s<sup>-1</sup>, it is rather likely that friction velocities under the ice are frequently above the thresholds calculated above  
141 and that turbulent diffusion will dominate over molecular diffusion. Dalman et al. (2019) provided experimental evidence for  
142 such turbulent nutrient fluxes to the ice bottom, leading to increased chlorophyll concentrations at the bottom ice, in a strait  
143 with strong tidal currents. The mechanism treated here as turbulent diffusion seems analogous to “forced convection” in the  
144 lowermost parts of the brine network, which is driven by pressure differences caused by the shear under the sea ice (Neufeld,  
145 2008; Vancoppenolle et al., 2013).

## 146 **2.2 Implementation**

147 We used the Los Alamos Sea Ice Model, which is managed by the CICE Consortium with an active forum  
148 (<https://bb.cgd.ucar.edu/cesm/forums/cice-consortium.146/>) and a git repository (<https://github.com/CICE-Consortium>). It  
149 includes two independent packages: CICE and Icepack. The former computes ice dynamic processes and the latter ice column  
150 physics and biogeochemistry. Their development is handled independently with respect to the GitHub repositories  
151 (<https://github.com/CICE-Consortium>). All the changes described below were implemented in two forks to the above  
152 repository, one for Icepack and another for CICE and they may be found in Duarte (2021a and b, respectively).

153 Our simulations may be run using only Icepack, since they are focused on ice column physics and biogeochemistry, without  
154 the need to consider ice dynamic processes. However, we used both CICE + Icepack together to allow for use of netCDF based  
155 input/output not included in Icepack. Therefore, we defined a 1D vertically resolved model with 1 snow layer and 15 ice layers  
156 and 5X5 horizontal cells. This is the minimum number of cells allowable in CICE due to the need to include halo cells (only  
157 the central “column” is simulated). Therefore, ice column physics and biogeochemistry were calculated by Icepack but CICE  
158 was the model driver. The input file (ice\_in) used in this study was included in our CICE fork and it lists all parameters used

159 in the model and described in Hunke et al. (2016), Jeffery et al. (2016), Duarte et al. (2017) and in Tables S1 and S2. Any  
160 changes in “default” parameters or any other model settings will be specified.

161 We made several modifications in CICE to allow using forcing time series collected during the Norwegian young sea ice (N-  
162 ICE2015) expedition (Granskog et al., 2018) and described in Duarte et al. (2017) (see Fig. 2 of the cited authors). These  
163 modifications were meant to allow reading of forcing data at higher frequencies than possible with the standard input  
164 subroutines in the CICE file ice\_forcing.F90.

165 When the dynamical component of CICE is not used,  $u^*$  is set to a minimum value instead of being calculated as a function of  
166 ice-ocean shear stress (Hunke et al., 2015). Duarte et al. (2017) implemented shear calculations from surface current velocities  
167 (one of the models forcing functions) irrespective of the use of the CICE dynamics code. These modifications were also  
168 incorporated in the current model configuration so that shear can be used to calculate friction velocity and, thereafter, influence  
169 heat and tracer/nutrient exchanges, following Eqs. (3) and (4) and parameters described in McPhee et al. (2008). When the  
170 parameter `kdyn` is set to zero in `ice_in`, ice dynamics is not computed, but shear is calculated in the modified subroutine  
171 `icepack_step_therm1`, file `icepack_therm_vertical.F90`. If `kdyn` is not zero, these calculations are ignored since shear is already  
172 calculated in the dynamical part of the CICE code.

173 A Boolean parameter (`Bottom_turb_mix`) was added to the input file, which is set to “false” or “true” when the standard  
174 molecular diffusion approach or the new turbulent based diffusion approach is used, respectively. Another Boolean parameter  
175 (`Limiting_factors_file`) was added to the `ice_in` file. When set to “true” limiting factor values for light, temperature, nitrogen,  
176 and silicate are written to a text file every model timestep. These are calculated by Icepack biogeochemistry, according to  
177 Jeffery et al. (2016), but there is no writing-output option in the standard code.

### 178 **2.3 Model simulations**

179 Simulations were run for a refrozen lead (RL) without snow cover and for second-year sea ice (SYI) with ~40 cm snow cover  
180 monitored in April-June during the N-ICE2015 expedition (Granskog et al., 2018 and Fig. 1 of Duarte et al. 2017). Details on  
181 model forcing with atmospheric and oceanographic data collected during the N-ICE2015 expedition, including citations and  
182 links to the publicly available datasets are given in Fig. 2 and section 3 of Duarte et al. (2017) and in the Supporting information  
183 file. These data sets include wind speed, air temperature, precipitation, and specific humidity (Hudson et al., 2015); incident  
184 surface short and longwave radiation (Hudson et al., 2016); ice temperature and salinity (Gerland et al., 2017); sea surface  
185 current velocity, temperature, salinity and heat fluxes from a turbulence instrument cluster (TIC) (Peterson et al., 2016); sea  
186 surface nutrient concentrations (Assmy et al., 2016) and sea ice biogeochemistry (Assmy et al., 2017). Ocean forcing is based  
187 on measurements within the surface 2 meters which provide the boundary condition for the sea ice model. Model forcing files  
188 may be found in Duarte (2021c).

189 Refrozen lead simulations started with zero ice, whereas Second Year Ice Simulations started with initial conditions described  
190 in the Supporting information file (Table S3).

191 We ran simulations with the standard formulations for biogeochemical processes described in Jeffery et al. (2016) and settings  
192 described in Duarte et al. (2017), using mushy thermodynamics, vertically resolved biogeochemistry, and including: freezing,  
193 flushing, brine mixed length and molecular diffusion within the ice and at the interface between the ocean and the sea ice as  
194 nutrient exchange mechanisms (Jeffery et al., 2011, 2016). We contrasted the above simulations against others that replaced  
195 brine molecular and mixed length diffusion of nutrients at the interface between the ocean and the sea ice with diffusion driven  
196 by current velocity shear (Table 1), calculated similar to heat exchanges, and following the parameterization described in  
197 McPhee et al. (2008) and detailed above (equations 2 - 7). This contrast provides insight into the effects of velocity shear on  
198 nutrient diffusion, ice algal production ( $\text{mg C m}^{-2} \text{d}^{-1}$ ), chlorophyll standing stocks ( $\text{mg Chl } a \text{ m}^{-2}$ ) and vertical distribution of  
199 chlorophyll concentration ( $\text{mg Chl } a \text{ m}^{-3}$ ) [note that CICE model output for algal biomass in  $\text{mmol N m}^{-3}$  was converted to  $\text{mg}$   
200  $\text{Chl } a \text{ m}^{-3}$  as in Duarte et al. (2017), using  $2.1 \text{ mg Chl } a \text{ mmol N}^{-1}$  and following Smith et al. (1993)]. However, due to the  
201 concurrent effects of algal biomass exchange between the ocean and ice, such a contrast is not enough to explicitly test our  
202 hypothesis and conclude about the effects of turbulent-driven nutrient supply on ice algal nutrient limitation. Therefore,  
203 simulations were also run contrasting the same model setups, as described above, but restarting from similar algal standing  
204 stocks and vertical distributions within the ice and, switching off algal inputs from the water to the ice. This was done by  
205 nullifying the variable `algalN`, defining the ocean surface background ice algal concentration, in file `icepack_zbgc.F90`,  
206 subroutine `icepack_init_ocean_bio` and in the restart files. In the case of the RL simulations that started with zero ice, first a  
207 simulation was run until the 12 May, and then the obtained ice conditions were used to restart new simulations without algal  
208 inputs from the ocean (`algalN = 0 mmol N m-3`). This way, when the simulations restarted, there was already an ice algal  
209 standing stock necessary for the modelling experiments developed herein. The SYI simulations were, by default, “restart  
210 simulations”, beginning with observed ice physical and biogeochemical variables. Therefore, there was already an algal  
211 standing stock in the ice from the onset (Text S1 and Table S3).

212 McPhee et al. (2008) estimated different values for  $\alpha_s$ , depending on whether the sea ice is growing (highest value) or melting  
213 (lowest value) (Table 1). When running simulations for the RL, in some cases, we used only the minimum or the maximum  
214 values for  $\alpha_s$ , to allow for a more extreme contrast between molecular and turbulent diffusion parameterizations. This was done  
215 since the former value will tend to minimize differences, whereas the latter will tend to emphasize them. We also completed  
216 simulations for the RL and for SYI changing between the maximum and the minimum values of  $\alpha_s$ , when ice was growing or  
217 melting, respectively, and following McPhee et al. (2008) (see Table 1 for details). This parameterization with a variable  $\alpha_s$ ,  
218 is likely the most realistic one, accounting for double diffusion during ice melting (MCPhee et al., 2008).

219 Apart from contrasting the way bottom-ice exchanges of nutrients were calculated, some simulations contrasted different  
220 parameters related to silicate limitation (Table 1). This approach follows Duarte et al. (2017), where simulations were tuned  
221 by changing the Si:N ratio and the half saturation constant for silicate uptake because silicate limitation was leading to an  
222 underestimation of algal growth. From this exercise we were able to assess if such tuning was still necessary after implementing  
223 turbulent diffusion at the interface between the ocean and the sea ice, driven by velocity shear. Moreover, we repeated

224 simulations with varying snow heights to further investigate the interplay between light and nutrient limitation under  
225 contrasting nutrient diffusion parameterizations (Table 1).

226

227

228

229

230

231

232

233

234

235



236 **Table 1. Model simulations. Refrozen lead (RL) simulation RL\_Sim1 corresponds to RL\_Sim5 described in Duarte et al. (2017) - the simulation leading**  
 237 **to a best fit to the observations in that study. The remaining RL simulations 2 – 5 differ from RL\_Sim1 in using turbulent diffusion at the interface between**  
 238 **the ocean and the sea ice for nutrients in a comparable way as it is calculated for heat and driven by velocity shear. Moreover, RL\_Sim5 differs in the**  
 239 **concentration of ice algae in the water column that colonize the sea ice bottom (algalN) and in silicate limitation related parameters. These changes were**  
 240 **done iteratively to fit the model to the observations. In RL\_Sim2 and RL\_Sim3 the maximum ( $\alpha_s=0.006$ ) and the minimum ( $\alpha_s=0.006/70=8.6 \cdot 10^{-5}$ ) values**  
 241 **recommended by McPhee et al. (2008), respectively, are used throughout the simulations, to provide extreme case scenarios for comparison with RL\_Sim1.**  
 242 **In RL\_Sim4,  $\alpha_s=8.6 \cdot 10^{-5}$  when ice is not growing and 0.006 otherwise, as recommended by McPhee et al. (2008), to account for double diffusive processes**  
 243 **during ice melting that slow down mass exchanges. The remaining RL simulations (RL\_Sim6-9) are like the previous ones (RL\_Sim1-4, respectively),**  
 244 **except for algalN that was set to zero mmol N m<sup>-3</sup>, and all simulations were restarted with the same values for all variables. Therefore, simulations 6 – 9**  
 245 **may differ only from 13 May 2015, when they were restarted. Second year ice simulation SYI\_Sim\_1 is based on Duarte et al. (2017) SYI\_Sim4 but without**  
 246 **algal motion. SYI\_Sim2 and SYI\_Sim3 use turbulent diffusion at the interface between the ocean and the sea ice. The former uses a decreased half**  
 247 **saturation constant for silicate uptake, just like SYI\_Sim1, whereas the latter uses the standard CICE value. The remaining SYI simulations (SYI\_Sim4**  
 248 **and 5) are like SYI\_Sim1 and 2, except for algalN that was set to zero. Simulations SYI\_Sim1 and SYI\_Sim2 were repeated but with different initial snow**  
 249 **thickness of 30, 20 and 15 cm to further investigate the interplay between light and silicate limitation (see text). Modified parameter values from one**  
 250 **simulation to the next are marked in bold, separately for RL and SYI simulations. Modified parameters are based on literature ranges [e.g. Brzezinski**  
 251 **(1985) and Hegseth (1992), for ratio\_Si2N\_diatoms, Nelson and Treguer (1992), for K\_Sil\_diatoms], Urrego-Blanco et al. (2016), for R\_snw], or on**  
 252 **previous model calibration work (Duarte et al., 2017). Parameters values were modified in the model input file ice\_in, except for algalN and  $\alpha_s$ , that are**  
 253 **hard-coded.**

Simulations	Modified parameters (bold types below indicate the parameter abbreviation used in Icepack)					
	Silica to nitrogen ratio in diatoms ( <b>ratio_Si2N_diatoms</b> )	Half saturation constant for silicate uptake ( <b>K_Sil_diatoms</b> , mM Si)	Ice algal concentration in the water ( <b>algalN</b> , mM N)	Boolean to define the usage of either molecular (0) or turbulent diffusion (1) ( <b>Bottom_turb_mix</b> )	Interface salt/nutrient turbulent exchange coefficient ( $\alpha_s$ )	Sigma coefficient for snow grain ( <b>R_snw</b> )
RL_Sim1	1.0	2.2	11 10 <sup>-4</sup>	0	-	1.5
RL_Sim2	1.0	2.2	11 10 <sup>-4</sup>	<b>1</b>	<b>0.006</b>	1.5
RL_Sim3	1.0	2.2	11 10 <sup>-4</sup>	1	<b>8.6 10<sup>-5</sup></b>	1.5
RL_Sim4	1.0	2.2	11 10 <sup>-4</sup>	1	<b>8.6 10<sup>-5</sup>-0.006</b>	1.5
RL_Sim5	<b>1.7</b>	<b>5.0</b>	<b>4 10<sup>-4</sup></b>	1	8.6 10 <sup>-5</sup> -0.006	1.5
RL_Sim6-9	As RL_Sim1-RL_Sim4, respectively		0	As RL_Sim1-RL_Sim4, respectively		
SYI_Sim1	1.0	2.2	11 10 <sup>-4</sup>	0	-	0.8

SYI_Sim2	1.0	2.2	$11 \cdot 10^{-4}$	<b>1</b>	<b><math>8.6 \cdot 10^{-5} - 0.006</math></b>	0.8
SYI_Sim3	1.0	<b>4.0</b>	$11 \cdot 10^{-4}$	1	$8.6 \cdot 10^{-5} - 0.006$	0.8
SYI_Sim4 and 5	As SYI_Sim1 and SYI_Sim2, respectively		0	As SYI_Sim1 and SYI_Sim2, respectively		

254

### 256 3. Results

257 The results of the simulations listed in Table 1 and presented below may be found in Duarte (2021d).

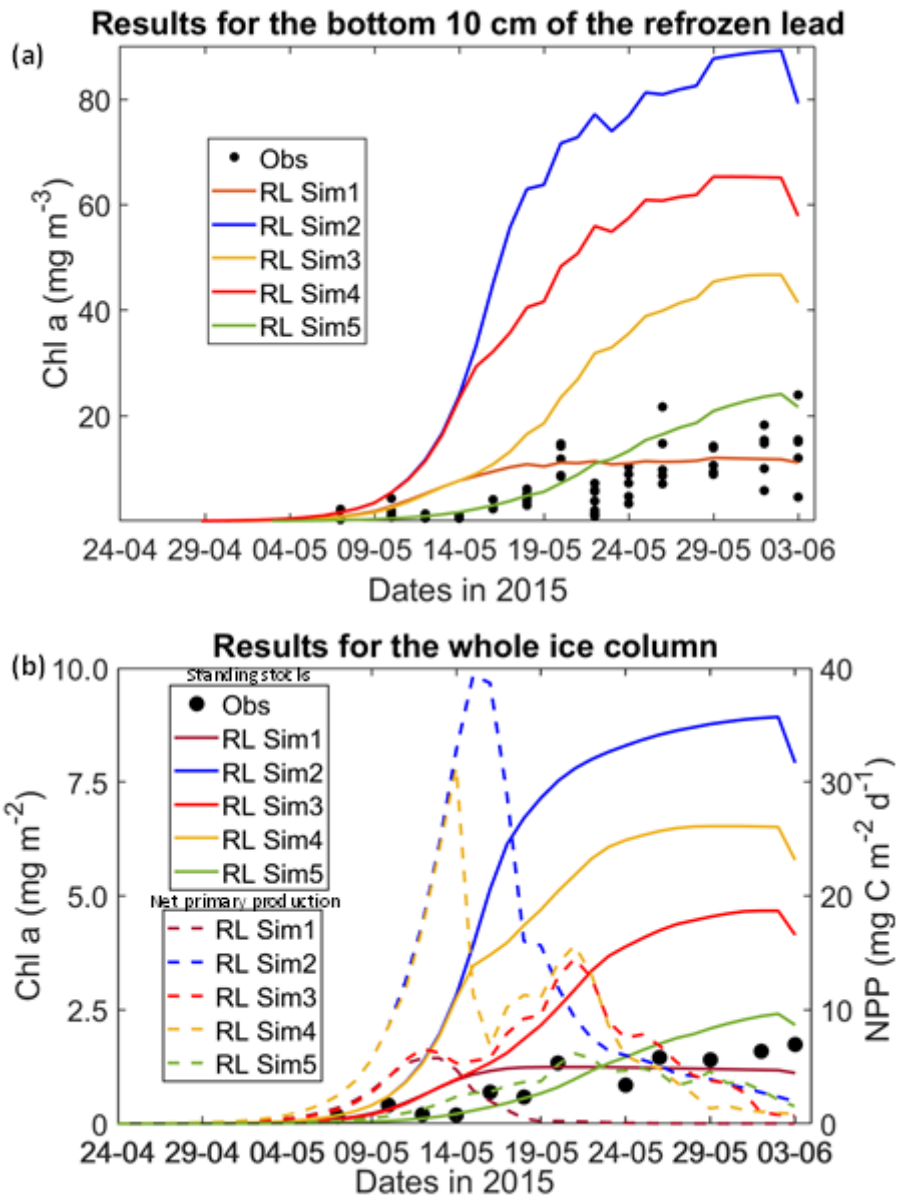
#### 258 3.1 Refrozen lead simulations

259 All simulations with turbulent diffusion (RL\_Sim2 – RL\_Sim5, Table 1), predict higher bottom chlorophyll *a* (*Chl a*)  
260 concentration than with the standard molecular diffusion formulation (RL\_Sim1) (Fig. 1a). Simulations RL\_Sim2 - 4 grossly  
261 overestimate observations. Simulation RL\_Sim3, using the lowest value for  $\alpha_s$ , is closer both to observations and to RL\_Sim1,  
262 as well as RL\_Sim5, with the latter having the same  $\alpha_s$  values of RL\_Sim4 but a half saturation constant for silicate limitation  
263 increased from its tuned value in Duarte et al. (2017) of 2.2  $\mu\text{M}$  to 5.0  $\mu\text{M}$  and algalN reduced (Table 1) to bring model results  
264 closer to observations. Patterns between simulations for the whole ice column and considering both standing stocks and net  
265 primary production, are similar to those observed for the bottom-ice (Fig. 1b). Algal biomass is concentrated at the bottom  
266 layers (Fig. 2). Concentrations in the layers located between the bottom and the top of the biogrid, defined by the vertical  
267 extent (brine height) of the brine network (green lines in the map plots) (Jeffery et al., 2011) are  $< 10 \text{ mg } Chl a \text{ m}^{-3}$ . Ice  
268 thickness, temperature and salinity profiles are extremely similar among these simulations (Figs. S1 and S2).

269 Results for the silicate and nitrogen limiting factors are based on brine concentrations. Limiting factors exhibiting lower values  
270 (more limitation) in RL simulations are silicate, followed by light (Figs. 3, S3 – S5). Limiting values for silicate range between  
271 zero (maximum limitation) and one (no limitation), with stronger limitation after May 13 in all simulations (Fig. 3). The most  
272 severe silicate limitation is for RL\_Sim1, where values drop to near zero around middle May. Despite the high average bottom  
273 *Chl a* concentration predicted in all simulations the bottom layer is where silicate limitation is less severe after May 13. This  
274 is more evident in simulations with turbulent bottom diffusion, where light limitation at the bottom-ice becomes more severe  
275 than silicate limitation around the end of May (Fig. S6).

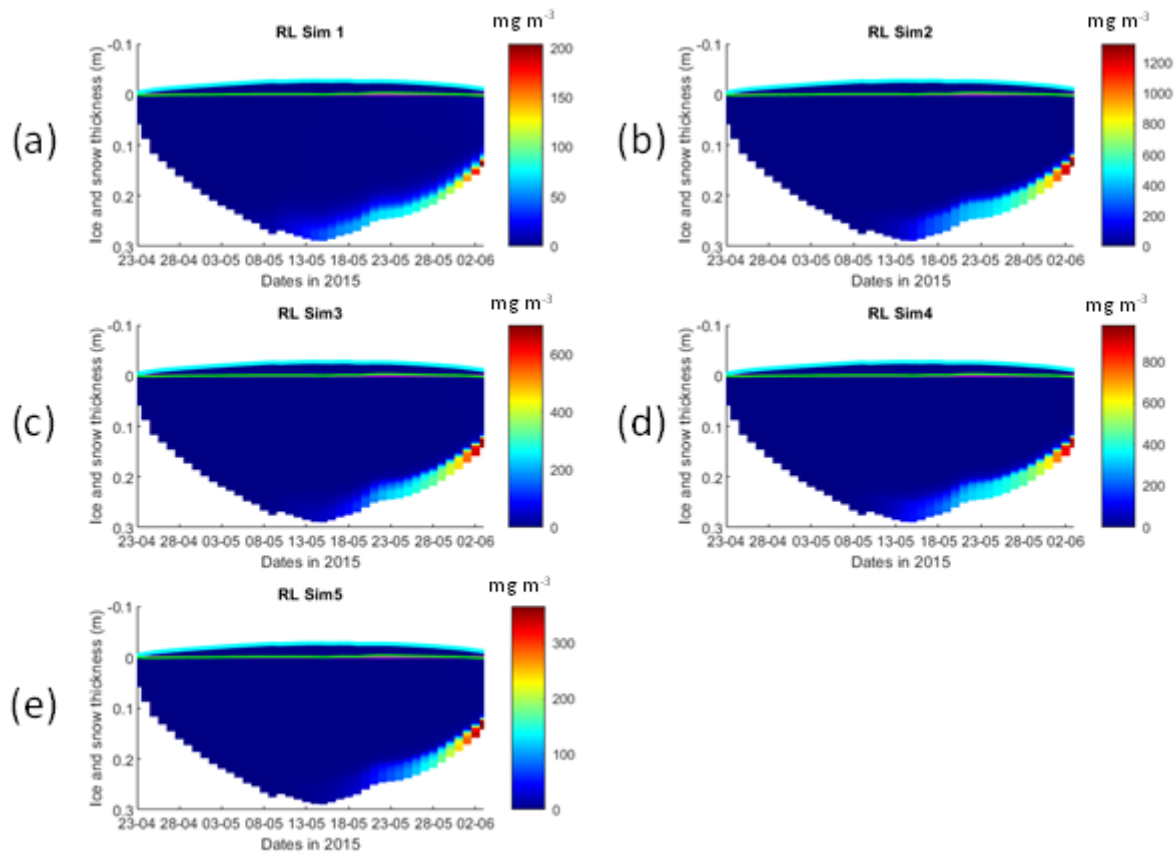
276 Results obtained with RL\_Sim6-9, without algal exchanges between the ocean and the ice (see Table 1), show similar patterns  
277 of those observed with RL\_Sim1-5, respectively (Fig. 4 versus Fig. 2, Fig. S9 versus Fig. 3, Figs. S7 and S8 versus Figs. S1  
278 and S2, Figs. S10 – S12 versus Figs. S3 – S5).

279 Interface diffusivity (one of CICE diagnostic variables, corresponding to the diffusion coefficient between adjacent  
280 biogeochemical layers and between the bottom layers and the ocean) for simulations with turbulent exchanges ( $\alpha_s u^* H$ ) are up  
281 to two orders of magnitude higher at the bottom (diffusivity between the bottom layer and the ocean) than for the RL\_Sim1  
282 simulation with only molecular diffusion ( $D_m$ ) + the mixed length diffusion coefficient ( $D_{MLD}$ ) (refer 2.1 and Fig. 5).



284

285 **Figure 1. Daily averaged results for the refrozen lead (RL):** (a) Observed and modelled *Chl a* concentration values averaged for the  
 286 ice bottom 10 cm; (b) Observed and modelled *Chl a* standing stock (continuous lines) and modelled net primary production (NPP)  
 287 (dashed lines) for the whole ice column (refer to Table 1 for details about model simulations). Observations are the same presented  
 288 in Duarte et al. (2017).



289

290

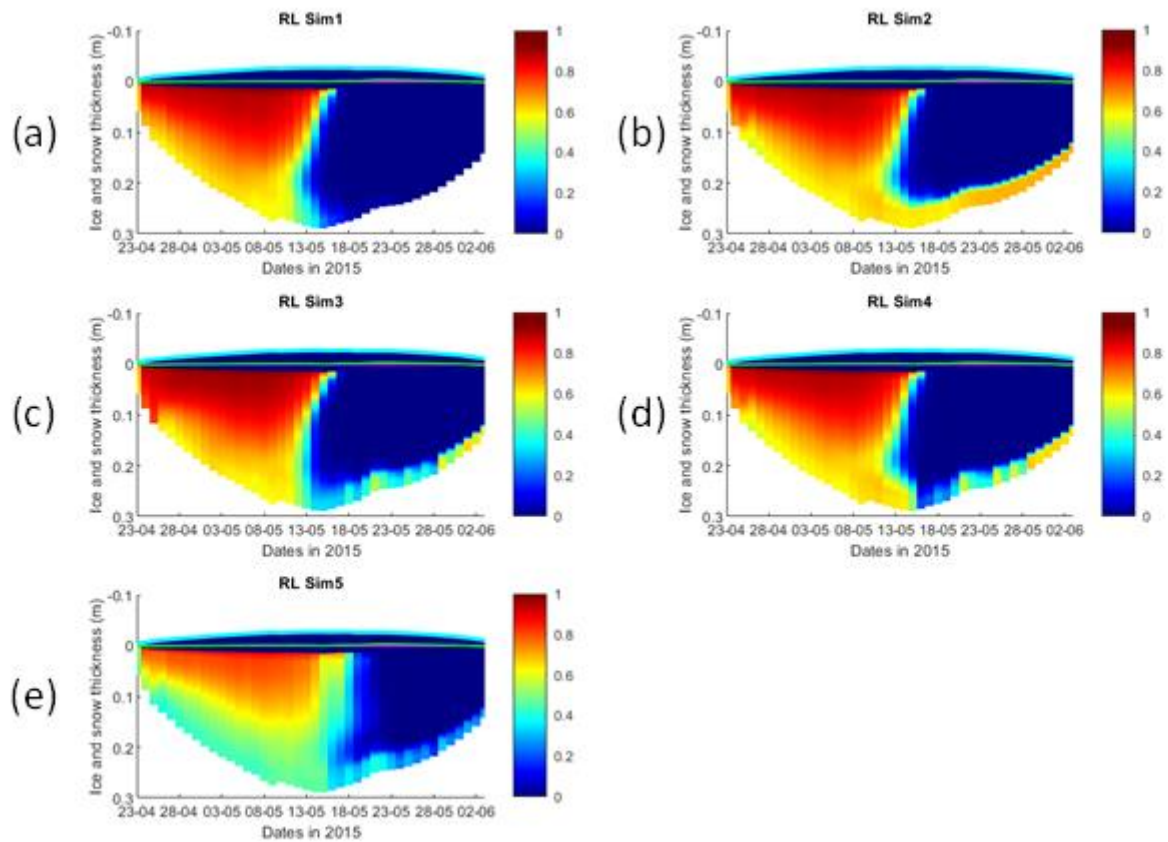
291

292

293

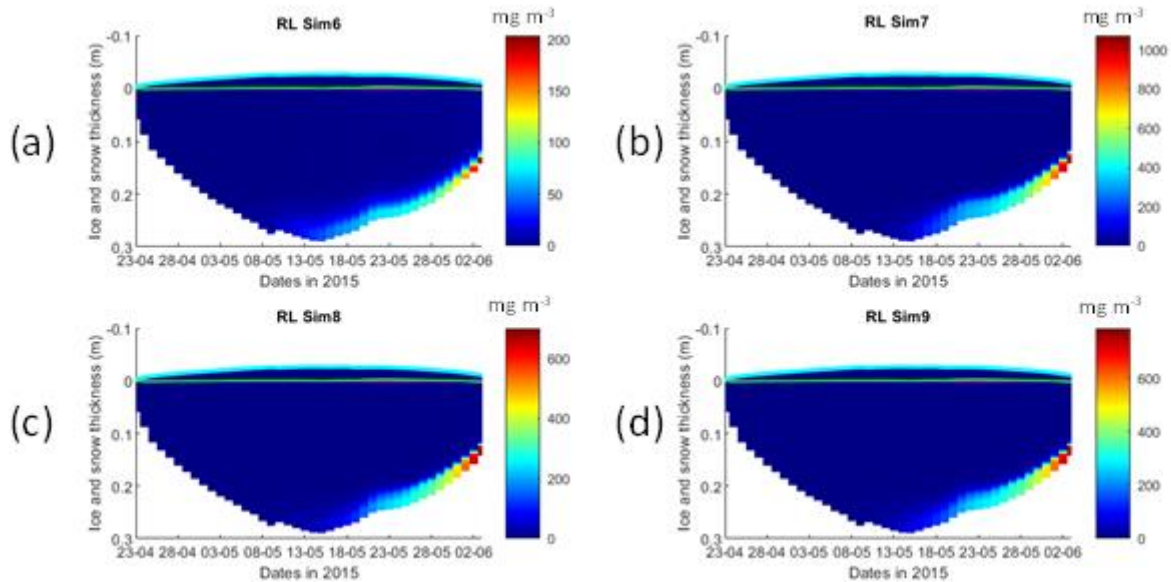
294

**Figure 2. Daily averaged results for the refrozen lead (RL) simulations 1 - 5: Simulated evolution of ice algae *Chl a* as a function of time and depth in the ice (note the colour scale differences between the various panels). Ice thickness is given by the distance between the upper and the lower limits of the maps. The upper regions of the graphs, above the green line with zero values, are above the CICE biogrid and have no brine network. The magenta line, partly covered by the green line, represents sea level. Refer to Table 1 for details about model simulations.**



295

296 **Figure 3. Daily averaged results for the refrozen lead (RL) simulations 1 - 5: Simulated evolution of silicate limitation (one means**  
 297 **no limitation and zero is maximal limitation), as a function of time and depth in the ice. Ice thickness is given by the distance between**  
 298 **the upper and the lower limits of the maps. The upper regions of the graphs, above the green line with zero values, are above the**  
 299 **CICE biogrid and have no brine network. The magenta line, partly covered by the green line, represents sea level. Refer to Table 1**  
 300 **for details about model simulations.**



301

302

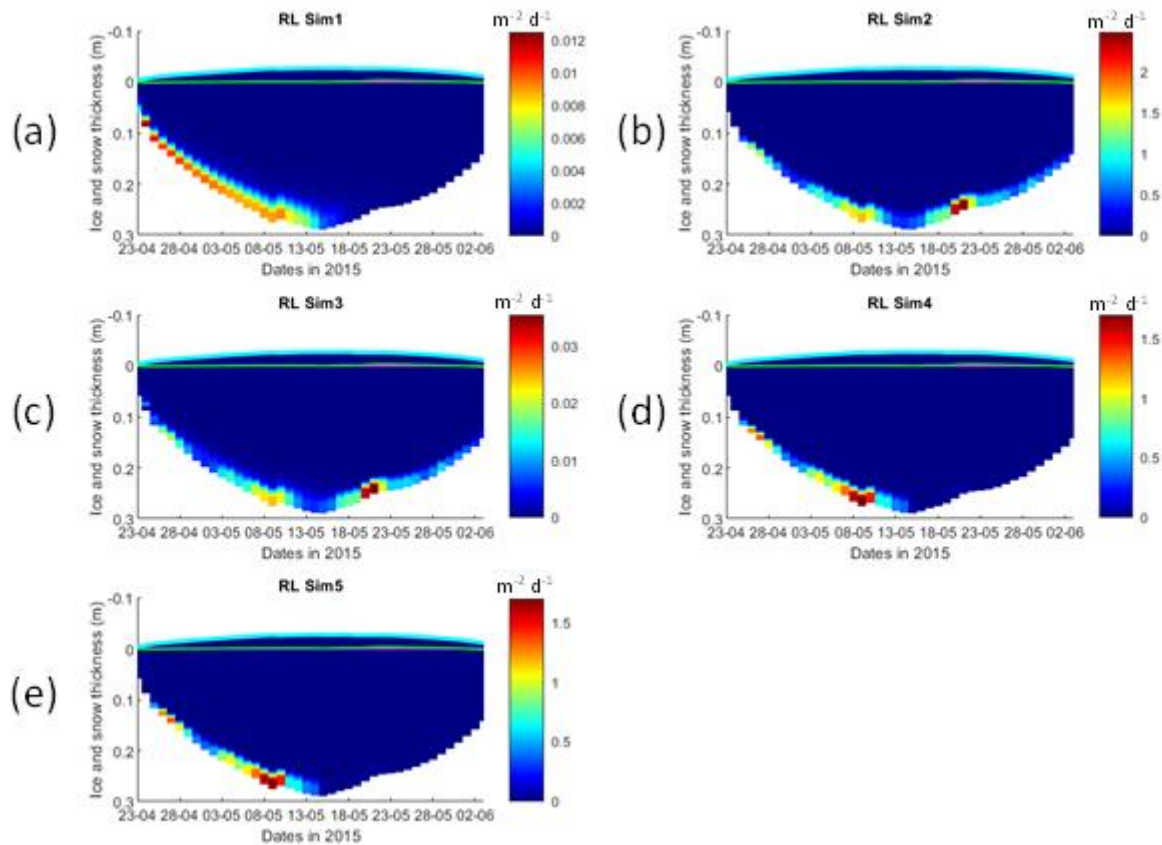
303

304

305

306

**Figure 4. Daily averaged results for the refrozen lead (RL) simulations 6 - 9: Simulated evolution of ice algae *Chl a* as a function of time and depth in the ice (note the colour scale differences between the various panels). Ice thickness is given by the distance between the upper and the lower limits of the maps. The upper regions of the graphs, above the green line with zero values, are above the CICE biogrid and have no brine network. The magenta line, partly covered by the green line, represents sea level. Refer to Table 1 for details about model simulations.**



307

308 **Figure 5. Daily averaged results for the refrozen lead (RL) simulations 1-5: Simulated evolution of interface diffusivity as a function**  
 309 **of time and depth in the ice (note the colour scale differences between the various panels). Ice thickness is given by the distance**  
 310 **between the upper and the lower limits of the maps. The upper regions of the graphs, above the green line with zero values, are**  
 311 **above the CICE biogrid and have no brine network. The magenta line represents sea level. Refer to Table 1 for details about model**  
 312 **simulations.**

313

### 314 3.2 Second year ice simulations

315 Simulations with turbulent diffusion (SYI\_Sim2 and 3), predict only slightly higher standing stocks and net primary production  
 316 than with the standard molecular diffusion formulation (SYI\_Sim1) (Fig. 6). The visual fit to the standing stock observations  
 317 is comparable between the various simulations. Changing the half saturation constant for silicate limitation from 2.2 to 4.0  $\mu\text{M}$   
 318 has no impact on model results. This is confirmed by analysing the evolution of *Chl a* concentration as a function of time and  
 319 depth in the ice (Fig. 7), with only minor differences being apparent towards the end of the simulation, when *Chl a* increases



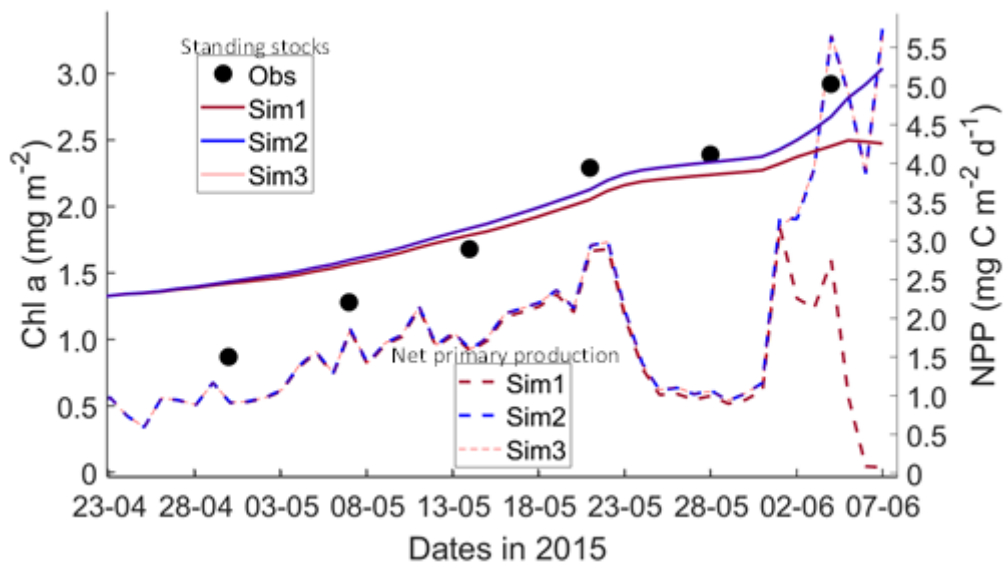
320 at the bottom layers in the simulations with turbulent diffusion (SYI\_Sim 2 and 3). Ice thickness, temperature and salinity  
321 profiles are extremely similar among these simulations (Fig. S13).

322 The dominant limiting factor in these simulations is light, followed by silicate (compare Fig. 8a, c and e with 8b, d and f and  
323 with Fig. S14). Light limitation is less severe after the onset of snow and ice melting at the beginning of June. Silicate limitation  
324 is very strong above the bottom ice. Nitrogen limitation is highest at a depth range between ~0.4 ~0.7 m below the ice top,  
325 with a large overlap with the depth range where a *Chl a* maximum is observed (Fig. 7). Maximal *Chl a* concentration predicted  
326 for the RL\_Sim1 and RL\_Sim5 simulations - those closer to observations - are two orders of magnitude higher than those  
327 predicted for SYI (Fig. 2a and e versus Fig. 7). However, standing stocks predicted for RL\_Sim1 and RL\_Sim5 simulations  
328 are smaller than for SYI simulations, as confirmed by the observations (Figs. 1b and 6). Opposite to what was described for  
329 the RL simulations, silicate limitation becomes more severe than light limitation at the bottom layer only in SYI\_Sim\_1, at the  
330 beginning of June, close to the end of the simulation (Fig. S15).

331 Results obtained without algal exchanges between the ocean and the ice (SYI\_Sim4 and 5, see Table 1), show the same patterns  
332 of those observed with SYI\_Sim1 and 2, respectively (Fig. 9 versus Fig. 7, Fig. S17 versus Fig. 8, Figs. S18 versus S14a - d  
333 and Figs. S16 versus S13a - d).

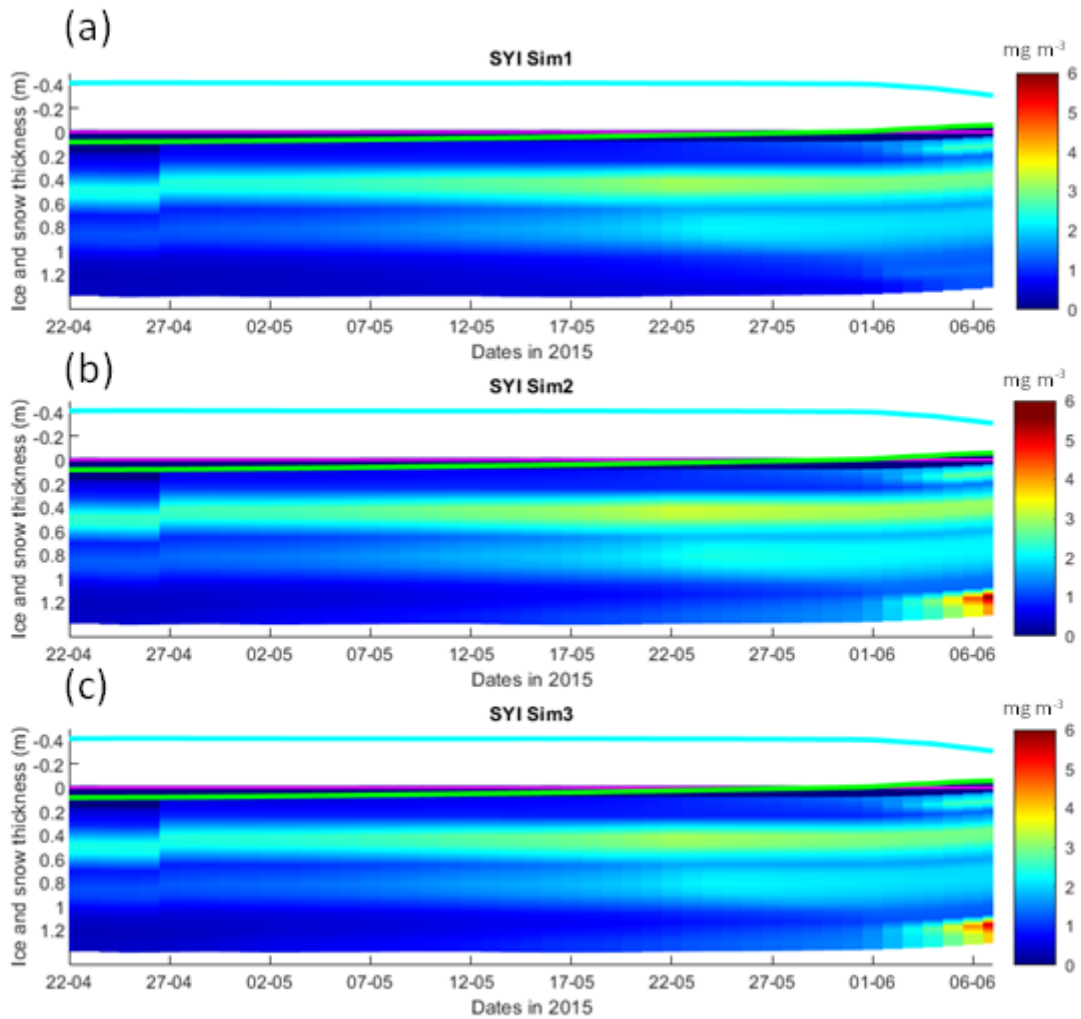
334 Interface diffusivity (one of CICE diagnostic variables, see above) for simulations with turbulent bottom exchanges are up to  
335 four orders of magnitude higher at the bottom ice than for simulations with only molecular diffusion (Fig. S19, showing a  
336 comparison between SYI\_Sim1 and SYI\_Sim2).

337 SYI\_Sim1 and 2 were repeated with varying snow thickness (Table 1 and Figs. 10 and 11). In the former simulation (Fig. 10a),  
338 as snow height decreases, there is a reduction in light limitation and a sharp increase in silicate limitation, overtaking light  
339 limitation (values becoming lower) as early as mid-May. In the latter simulation (Fig. 10b), light limitation prevails irrespective  
340 of snow height, except in the case of the lower snow height of 15 cm where silicate becomes more limiting towards the end of  
341 the simulation. With the decrease in snow height, there is an increase in *Chl a* concentration in all simulations. Highest values  
342 for SYI\_Sim2 are ~one order of magnitude larger than those for SYI\_Sim1. Moreover, the decrease in snow heights is followed  
343 by an earlier and more intense bottom ice algal bloom.



344

345 **Figure 6. Daily averaged results for second year ice (SYI) simulations 1 - 3: Observed [same data presented in Duarte et al. (2017)]**  
 346 **and modelled *Chl a* standing stock (continuous lines) and modelled net primary production (NPP) (dashed lines) for the whole ice**  
 347 **column (refer to Table 1 for details about model simulations).**



348

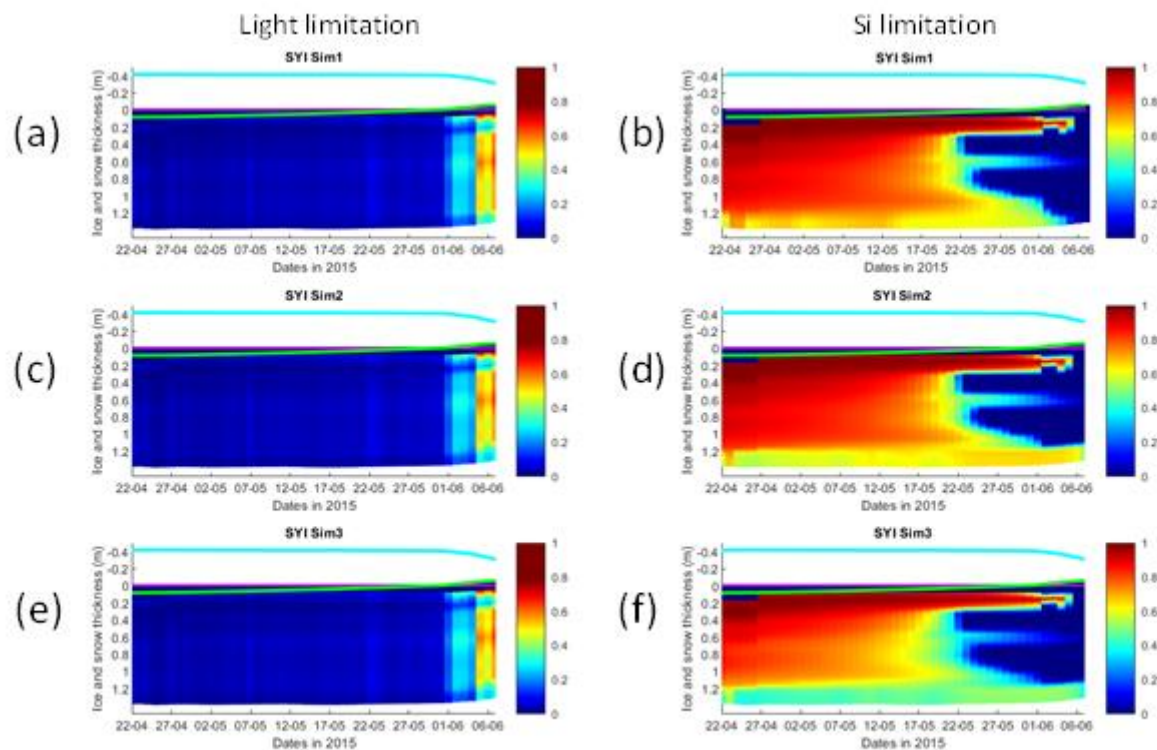
349

350

351

352

Figure 7. Daily averaged results for second year ice (SYI) simulations 1 - 3: Simulated evolution of ice algae *Chl a* as a function of time and depth in the ice. The upper regions of the graphs, above the green line with zero values, are above the CICE biogrid and have no brine network. The magenta line represents sea level, and the cyan line represents the top of the snow layer. Refer to Table 1 for details about model simulations.



353

354

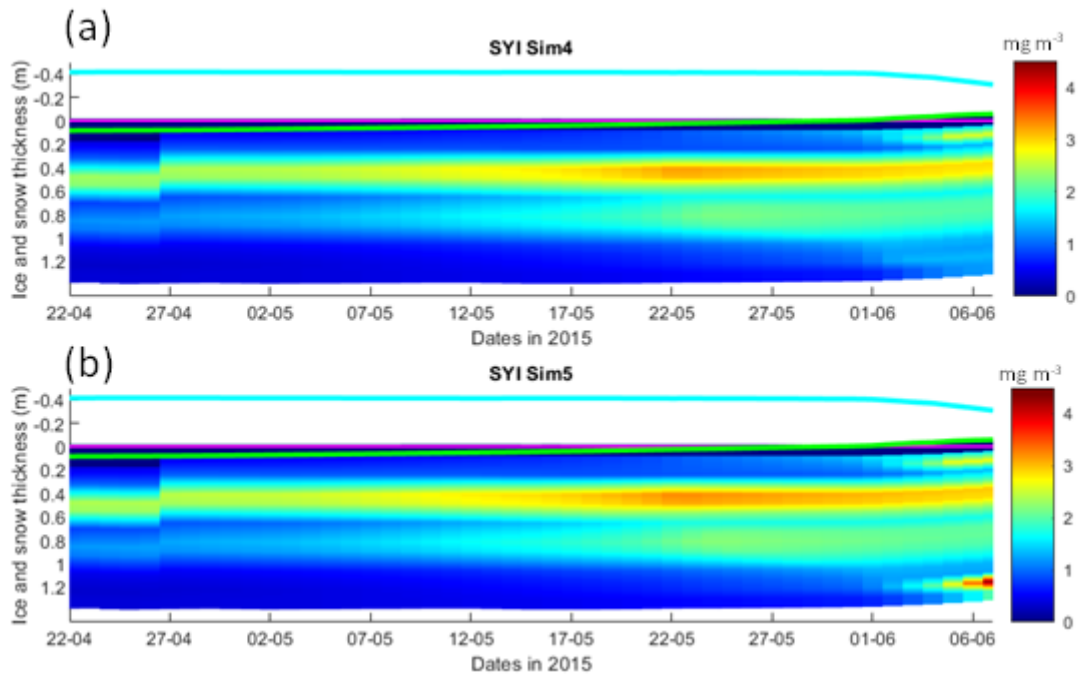
355

356

357

358

**Figure 8. Daily averaged results for second year ice (SYI) simulations 1 - 3: Simulated evolution of light (left panels) and silicate (right panels) limitation (one means no limitation and zero is maximal limitation), as a function of time and depth in the ice. The upper regions of the graphs, above the green line with zero values, are above the CICE biogrid and have no brine network. The magenta line represents sea level, and the cyan line represents the top of the snow layer. Refer to Table 1 for details about model simulations.**



359

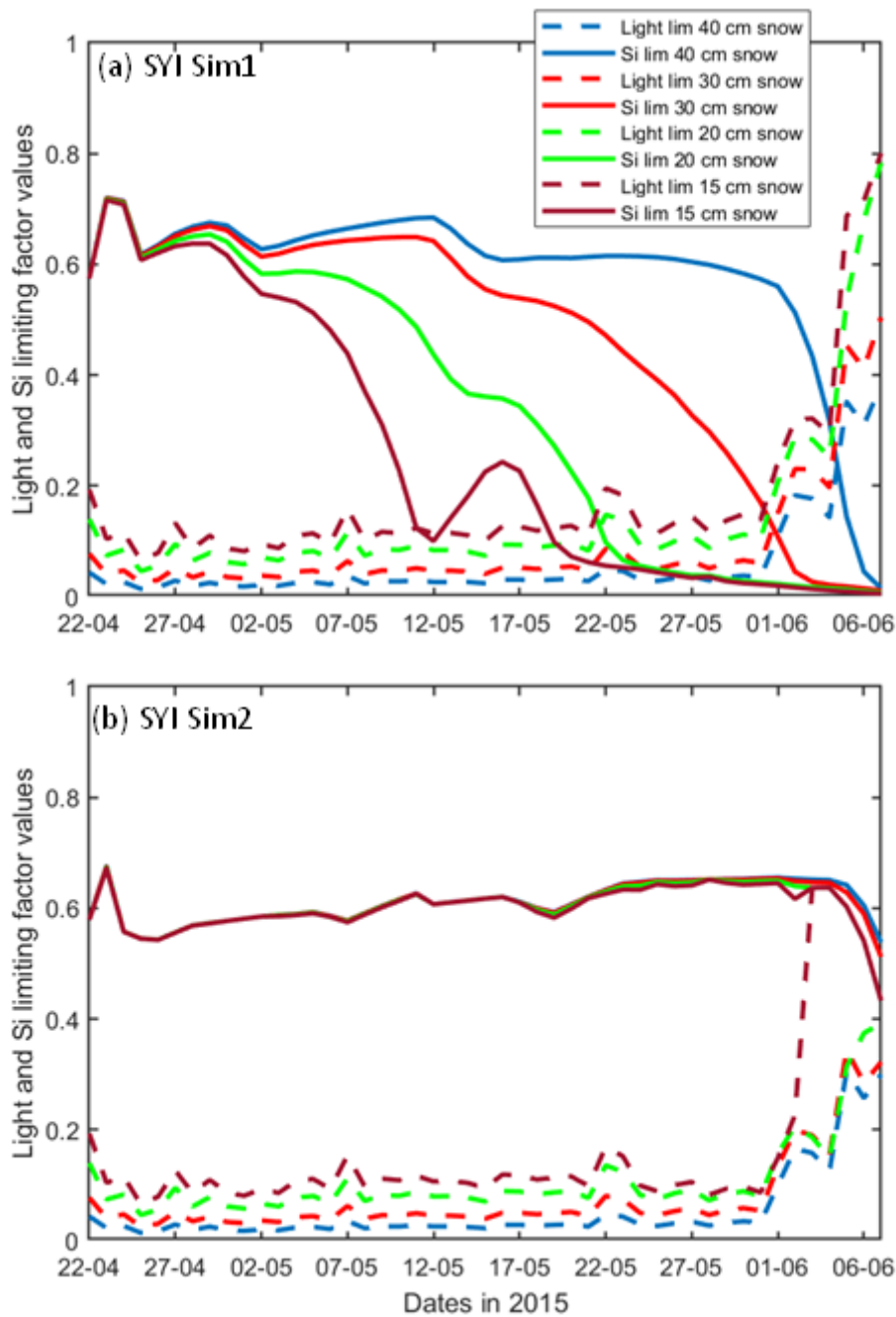
360

361

362

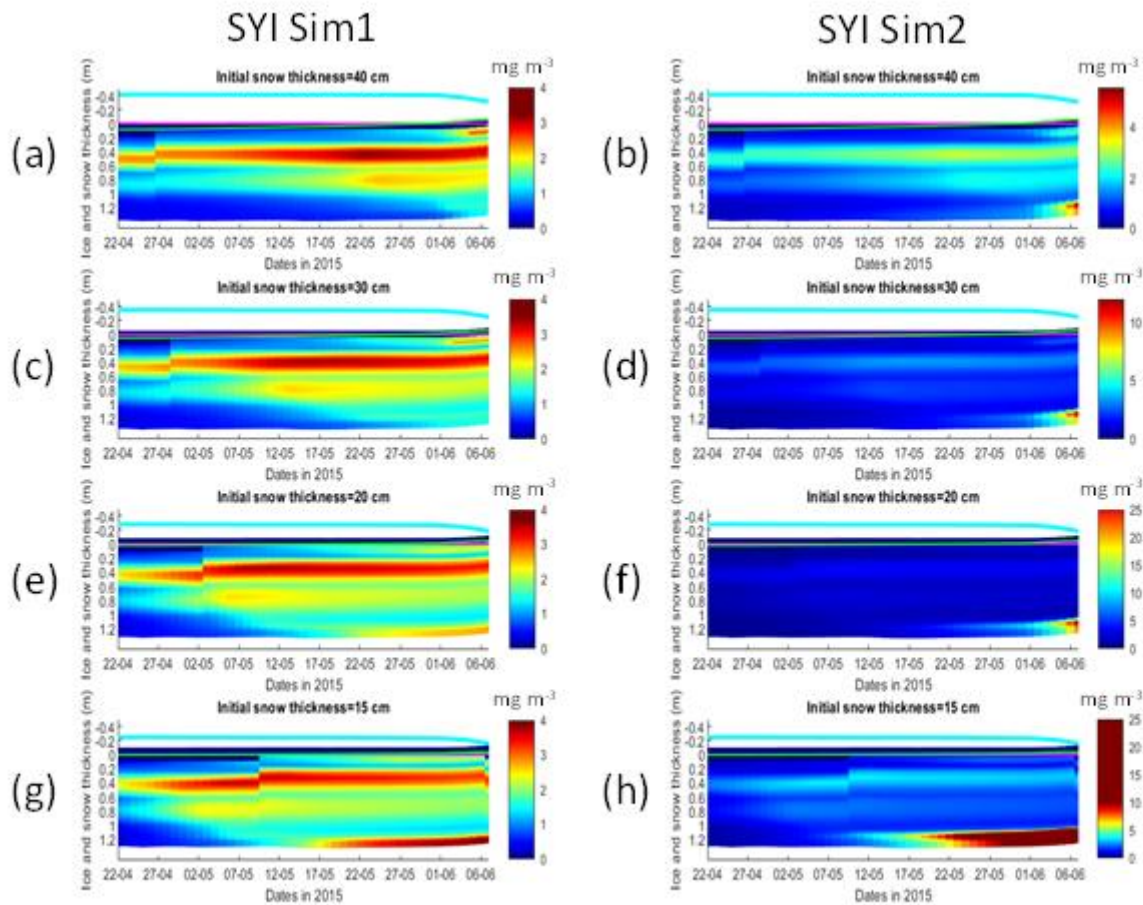
363

**Figure 9. Daily averaged results for second year ice (SYI) simulations 4 and 5: Simulated evolution of ice algae *Chl a* as a function of time and depth in the ice. The upper regions of the graphs, above the green line with zero values, are above the CICE biogrid and have no brine network. The magenta line represents sea level, and the cyan line represents the top of the snow layer. Refer to Table 1 for details about model simulations.**



364

365 **Figure 10. Daily averaged results for the second-year ice (SYI) simulations 1 (a) and 2 (b) starting with a snow depth of 40 (default**  
 366 **simulation), 30, 20 and 15 cm: Simulated evolution of light (dashed lines) and silicate (continuous lines) limitation (one means no**  
 367 **limitation and zero is maximal limitation), as a function of time at the ice bottom layer (one means no limitation). Refer to Table 1**  
 368 **for details about model simulations.**



369

370 **Figure 11. Daily averaged results for second year ice (SYI) simulations 1 (left panels) and 2 (right panels) starting with a snow depth**  
 371 **of 40 (default simulation), 30, 20 and 15 cm: Simulated evolution of ice algae *Chl a* as a function of time and depth in the ice. The**  
 372 **upper regions of the graphs, above the green line with zero values, are above the CICE biogrid and have no brine network. The**  
 373 **magenta line represents sea level, and the cyan line represents the top of the snow layer. Refer to Table 1 for a description of model**  
 374 **simulations.**

#### 375 4. Discussion

376 The results obtained in this study support the initial hypothesis, showing that considering the role of velocity shear on turbulent  
 377 nutrient exchanges between the ocean and the sea ice, formulated in a way consistent with heat exchanges, leads to a reduction  
 378 in nutrient limitation that supports a significant increase in ice algal net primary production and *Chl a* biomass accumulation  
 379 in the bottom ice layers, when production is nutrient limited. Therefore, our results are in line with empirical evidence provided  
 380 by Cota et al. (1987) and Dalman et al. (2019) but, to the best of our knowledge, experimental evidence from properly designed  
 381 experiments is still lacking to test our hypothesis. Moreover, our results do not imply necessarily that experiments carried out

382 with other sea-ice models would render the same trends. The implementation of turbulent mixing considerably relieved silicate  
383 limitation in the RL simulations, leading to an increase in NPP, in the duration of the algal growth period, in bottom *Chl a*  
384 concentration and in-ice light absorption, increasing light limitation due to shelf-shading [in the CICE model, optical ice  
385 properties are influenced by ice algal concentrations (Jeffery et al., 2016)].

386 In the N-ICE2015 biogeochemical dataset (Assmy et al., 2016), the median of dissolved inorganic nitrogen to silicate ratios in  
387 all surface and subsurface water masses, is above 1.7 (unpublished data), which is the upper limit for the nitrogen to silicate  
388 ratio for polar diatoms (e.g. Takeda, 1998; Krause et al. 2018). Therefore, it can be expected that, in the region covered by the  
389 N-ICE2015 expedition, silicate is more limiting than nitrogen for the production yields of the pennate diatoms characteristic  
390 of the bottom-ice communities [the dominant algal functional group in bottom ice, e.g. Leu et al. (2015), van Leeuwe et al.  
391 (2019)]. Elsewhere in the Arctic the opposite may be true, considering nitrate and silicate concentrations presented in Leu et  
392 al. (2015) and the number of process studies documenting such limitation [e.g., Campbell et al. (2016)]. However, the  
393 conclusions taken here about the effects of turbulent mixing are independent of the limiting nutrient.

394 Implementing turbulent diffusion between the ice and the ocean has obvious implications for model tuning. Our results for the  
395 RL show that with this formulation it was necessary to increase the half saturation constant for silicate uptake and to reduce  
396 the ocean concentration of algal nitrogen (algalN), reducing the colonization of bottom ice by ice algae, to obtain *Chl a* values  
397 comparable to those observed (RL\_Sim5). Therefore, whereas Duarte et al. (2017) had to reduce silicate limitation to improve  
398 the fit between modelled and observational data, the opposite approach was required when using turbulent diffusion in line  
399 with results reported in Lim et al. (2019) for Antarctic sea ice diatoms. This is an example of how one can get good model  
400 results by the wrong reasons with difficult to predict consequences on model forecasts under various scenarios.

401 In the SYI case, only a minor increase in bottom *Chl a* concentration was observed towards the end of simulations SYI\_Sim\_2  
402 and SYI\_Sim\_3, when light limitation due to the thick snow cover was relieved by snow melt. Silicate limitation was not as  
403 severe as in SYI\_Sim\_1, due to greater bottom exchanges in the former simulations. The importance of snow cover in  
404 controlling ice algal phenology has been stressed before [e.g., Campbell et al. (2015), Leu et al. (2015)].

405 Duarte et al. (2017) used the delta-Eddington parameter, corresponding to the standard deviation of the snow grain size  
406 ( $R_{\text{snow}}$ ) (Urrego-Blanco et al., 2016), to tune model predicted shortwave radiation at the ice bottom. However, there was  
407 still a positive shortwave model bias in June. Therefore, our conclusion about the main limiting role of light in SYI is  
408 conservative. Moreover, in part of SYI cores sampled during the N-ICE2015 expedition, in the period covered by our  
409 simulations, with an unusually high snow thickness (~40 cm), there was no *Chl a* bottom maximum (Duarte et al., 2017; Olsen  
410 et al., 2017).

411 The dominant role of light limitation in SYI was confirmed in the simulations with reduced snow thickness and alleviated light  
412 limitation, with a bottom-ice algal *Chl a* maximum emerging earlier at snow thickness  $\leq 20$  cm. The reduction of snow  
413 thickness had a much larger effect in increasing *Chl a* concentration at the bottom layer when turbulent mixing was used, due  
414 to lower silicate limitation. Reducing snow thickness led to a relatively early shift from light to silicate limitation when we  
415 used molecular and mixed length diffusion, whereas this shift occurred only at the very end of the simulated period when we



416 used turbulent diffusion at the ice-ocean interface, driven by velocity shear, instead of molecular diffusion. The effects of  
417 different types of diffusion, upon reduction of the snow cover and the possible development of a bottom ice algal bloom, are  
418 critical aspects when simulating ice algal phenology and attempting to quantify the contribution of sea ice algae to Arctic  
419 primary production.

420 Simulated shear-driven turbulent diffusivities are up to four orders of magnitude higher than molecular + mixed length  
421 diffusivities at the bottom ice and the results presented herein emphasize their potential role in sea ice biogeochemistry. The  
422 number and intensity of Arctic winter storms has increased over the 1979–2016 period (Rinke et al., 2017; Graham et al.,  
423 2017) and the effect of more frequent and more intensive winter storms in the Atlantic Sector of the Arctic Ocean is a thinner,  
424 weaker, and younger snow-laden ice pack (Graham et al., 2019). Storms that occur late in the winter season, after a deep  
425 snowpack has accumulated, have the potential to promote ice growth by dynamically opening leads where new ice growth can  
426 take place. The young ice of the refrozen leads does not have time to accumulate a deep snow layer until the melting season,  
427 which could lead to light limitation of algal growth. All things considered, it can be expected that ongoing trends in the Arctic  
428 will lead to a release from light limitation in increasingly larger areas of the ice pack in late winter, which will lead to more  
429 likely nutrient limitation earlier in spring (e.g. Lannuzel et al. 2020). These effects will be further amplified under thinning of  
430 the snowpack as observed in western Arctic, and in the Beaufort and Chukchi seas, over the last decades (Webster et al., 2014).  
431 Therefore, properly parameterizing nutrient exchanges between the ice and the ocean in sea-ice biogeochemical models is of  
432 utmost importance to avoid overestimating nutrient limitation and thus underestimating sea ice algal primary production.

433 In existing sea-ice models there are “natural” differences between the way budgets for non-conservative tracers such as  
434 nutrients are closed compared to those of heat and salt, which are related to the biogeochemical sinks and sources (e.g., equation  
435 18 in Vancoppenolle et al., 2010), but also some “inconsistencies”, related with the way their transfers between the ocean and  
436 the ice are computed. Interestingly, some models (e.g., Jin et al., 2006, 2008 and Hunke et al., 2016) apply the diffusion  
437 equation to calculate exchanges across the bottom ice not only to dissolved tracers, but also to algal cells. This is to guarantee  
438 a mechanism of ice colonization by microalgae. However, the usage of the same coefficient for dissolved and particulate  
439 components creates significant uncertainty.

440 Molecular diffusion is a slow process compared with turbulent exchanges. This justifies the usage of diffusion coefficients  
441 which are much higher than molecular diffusivity, as in Jin et al. (2006), using a value of  $1.0 \cdot 10^{-5} \text{ m}^2 \text{ s}^{-1}$ , four orders of  
442 magnitude higher than the value indicated in Mann and Lazier (2005) –  $1.5 \cdot 10^{-9} \text{ m}^2 \text{ s}^{-1}$  – or the parameterization of diffusivity  
443 as a function of friction velocity as in Mortenson et al. (2017). The approach proposed herein, formulating bottom-ice nutrient  
444 exchanges in a way that is consistent with heat exchanges, provides a physically sound, consistent, and easy to implement  
445 alternative.

## 446 **5. Conclusions**

447 Considering the role of velocity shear on turbulent nutrient exchanges at the interface between the ocean and the ice in a sea-

448 ice biogeochemical sub-model, leads to a reduction in nutrient limitation and a significant increase in ice algal net primary  
449 production and *Chl a* biomass accumulation in the bottom-ice layers, when production is nutrient limited. The results presented  
450 herein emphasize the potential role of bottom-ice nutrient exchange processes, irrespective of brine dynamics and other  
451 physical-chemical processes, in delivering nutrients to bottom-ice algal communities, and thus the importance of properly  
452 including them in sea-ice models. The relevance of this becomes even more apparent considering ongoing changes in the  
453 Arctic icescape, with a predictable decrease in light limitation as ice becomes thinner and more fractured, with an expected  
454 reduction in snow cover.

#### 455 **Code availability**

456 The software code used in this study may be found at:

457 <https://doi.org/10.5281/zenodo.4675097> and <https://doi.org/10.5281/zenodo.4675021>

458 This code is in a fork derived from the CICE Consortium repository (<https://github.com/CICE-Consortium>).

459 The Consortium's codes are open-source with a standard 3-clause BSD license and are is under the following Copyright  
460 license, available at (<https://cice-consortium-cice.readthedocs.io/en/master/intro/copyright.html>)

461

#### 462 **Data availability**

463 Model forcing function files may be found at: <https://doi.org/10.5281/zenodo.4672176>

464 Results from model simulations described above, in the form of CICE daily netCDF history files iceh.\* may be found at:  
465 <http://doi.org/10.5281/zenodo.4672210>

466 There is one directory for each simulation, and it includes besides the historical files the input file (ice\_in) with the simulation  
467 parameters.

468

#### 469 **Authors contribution**

470 Pedro Duarte made the software changes, designed the experiments, performed the simulations and prepared the manuscript  
471 with contributions from all co-authors.

472 Philipp Assmy contributed to the writing of the manuscript.

473 Karley Campbell contributed to the writing of the manuscript.

474 Arild Sundfjord contributed to the writing of the manuscript and to funding acquisition.

475

#### 476 **Competing interests**

477 The authors declare that they have no conflict of interest.

478 **Acknowledgements**

479 This work has been supported by the Fram Centre Arctic Ocean flagship project “Mesoscale physical and biogeochemical  
480 modelling of the ocean and sea-ice in the Arctic Ocean” (project reference 66200), the Norwegian Metacenter for  
481 Computational Science application “NN9300K - Ecosystem modelling of the Arctic Ocean around Svalbard”, the Norwegian  
482 “Nansen Legacy” project (no. 276730) and the European Union’s Horizon 2020 research and innovation programme under  
483 grant agreement No 869154 (project FACE-IT). Contributions by K Campbell are supported by the Diatom ARCTIC project  
484 (NE/R012849/1;03F0810A), part of the Changing Arctic Ocean program, jointly funded by the UKRI Natural Environment  
485 Research Council and the German Federal Ministry of Education and Research (BMBF).

486 **References**

- 487 Arrigo, K. R., Kremer, J. N., and Sullivan, C. W.: A Simulated Antarctic Fast Ice Ecosystem, *J. Geophys. Res.*, 98, 17, 1993.
- 488 Assmy, P., Duarte, P., Dujardin, J., Fernández-Méndez, M., Fransson, A., Hodgson, R., Kauko, H., Kristiansen, S., Mundy, C.  
489 J., Olsen, L. M., Peeken, I., Sandbu, M., Wallenschus, J., Wold, A.: N-ICE2015 water column biogeochemistry [Data set],  
490 Norwegian Polar Institute, <https://doi.org/10.21334/npolar.2016.3ebb7f64>, 2017.
- 491 Assmy, P., Dodd, P. A., Duarte, P., Dujardin, J., Elliott, A., Fernández-Méndez, M., Fransson, A., Granskog, M. A., Hendry,  
492 K., Hodgson, R., Kauko, H., Kristiansen, S., Leng, M. J., Meyer, A., Mundy, C. J., Olsen, L. M., Peeken, I., Sandbu, M.,  
493 Wallenschus, J., Wold, A.: N-ICE2015 sea ice biogeochemistry [Data set], Norwegian Polar Institute,  
494 <https://doi.org/10.21334/npolar.2017.d3e93b31>, 2017.
- 495 Brzezinski, M. A.: The Si-C-N Ratio of Marine Diatoms - Interspecific Variability and the Effect of Some Environmental  
496 Variables, *J. Phycol.*, 21, 347-357, 1985.
- 497 Campbell, K., Mundy, C. J., Barber, D. G. and Gosselin, M.: Characterizing the sea ice algae chlorophyll a–snow depth  
498 relationship over Arctic spring melt using transmitted irradiance, *J. Mar. Sys.*, 147, 76-84, doi:  
499 <https://doi.org/10.1016/j.jmarsys.2014.01.008>, 2015.
- 500 Campbell, K., Mundy, C. J., Landy, J. C., Delaforge, A., Michel, C. and Rysgaard, S.: Community dynamics of bottom-ice  
501 algae in Dease Strait of the Canadian Arctic. *Prog. Oceanogr.*, 149, 27-39, doi: <http://dx.doi.org/10.1016/j.pcean.2016.10.005>,  
502 2016.
- 503 Carmack, E.: Circulation and Mixing in Ice-Covered Waters, in: *The Geophysics of Sea Ice. NATO ASI Series (Series B:  
504 Physics)*, edited by Untersteiner N. Springer, Boston, MA. 641-712, [https://doi.org/10.1007/978-1-4899-5352-0\\_11](https://doi.org/10.1007/978-1-4899-5352-0_11), 1986.
- 505 Cota, G. F., Prinsenberg, S. J., Bennett, E. B., Loder, J. W., Lewis, M. R., Anning, J. L., Watson, N. H. F., and Harris, L. R.:  
506 Nutrient Fluxes during Extended Blooms of Arctic Ice Algae, *J. Geophys. Res.-Oceans*, 92, 1951-1962, doi:  
507 10.1029/Jc092ic02p01951, 1987.
- 508 Cota, G. F., and Horne, E. P. W.: Physical Control of Arctic Ice Algal Production, *Mar. Ecol. Prog. Ser.*, 52, 111-121, doi:  
509 10.3354/meps052111, 1989.

510 Cota, G. F., and Sullivan, C. W.: Photoadaptation, Growth and Production of Bottom Ice Algae in the Antarctic, *J. Phycol.*,  
511 26, 399-411, doi: 10.1111/j.0022-3646.1990.00399.x, 1990.

512 Dalman, L. A., Else, B. G. T., Barber, D., Carmack, E., Williams, W. J., Campbell, K. , Duke, P. J., Kirillov, S., and Mundy,  
513 C. J.: Enhanced bottom-ice algal biomass across a tidal strait in the Kitikmeot Sea of the Canadian Arctic, *Elem. Sci. Anth.*, 7,  
514 doi: <https://doi.org/10.1525/elementa.361>, 2019.

515 Duarte, P., Meyer, A., Olsen, L. M., Kauko, H. M., Assmy, P., Rosel, A., Itkin, P., Hudson, S. R., Granskog, M. A., Gerland,  
516 S., Sundfjord, A., Steen, H., Hop, H., Cohen, L., Peterson, A. K., Jeffery, N., Elliott, S. M., Hunke, E. C., and Turner, A. K.:  
517 Sea ice thermohaline dynamics and biogeochemistry in the Arctic Ocean: Empirical and model results, *J. Geophys. Res.-*  
518 *Biogeosciences*, 122, 1632-1654, doi: 10.1002/2016JG003660, 2017.

519 Duarte, P.: CICE-Consortium/Icepack: Icepack with bottom drag, heat and nutrient turbulent diffusion (Version 1.1). Zenodo.  
520 <http://doi.org/10.5281/zenodo.4675021>, (2021a, April 9).

521 Duarte, P.: CICE-Consortium/CICE: CICE with bottom drag, heat and nutrient turbulent diffusion (Version 1.1). Zenodo.  
522 <http://doi.org/10.5281/zenodo.4675097>, (2021b, April 9).

523 Duarte, P.: The importance of turbulent ocean-sea ice nutrient exchanges for simulation of ice algal biomass and production  
524 with CICE6.1 and Icepack 1.2 - CICE forcing files (Version v1.0) [Data set]. Zenodo. <http://doi.org/10.5281/zenodo.4672176>,  
525 2021c.

526 Duarte, P.: The importance of turbulent ocean-sea ice nutrient exchanges for simulation of ice algal biomass and production  
527 with CICE6.1 and Icepack 1.2 - model simulations (Version v1.0) [Data set]. Zenodo. <http://doi.org/10.5281/zenodo.4672210>,  
528 2021c.

529 Gerland, S., Granskog, M. A., King, J, Rösel, A.: N-ICE2015 Ice core physics: temperature, salinity and density [Data set],  
530 Norwegian Polar Institute, <https://doi.org/10.21334/npolar.2017.c3db82e3>, 2017.

531 Gosselin, M., Legendre, L., Demers, S., and Ingram, R. G.: Responses of Sea-Ice Microalgae to Climatic and Fortnightly Tidal  
532 Energy Inputs (Manitounuk Sound, Hudson-Bay), *Can. J. Fish. Aquat. Sci.*, 42, 999-1006, doi: 10.1139/f85-125, 1985.

533 Graham, R. M., Rinke, A., Cohen, L., Hudson, S. R., Walden, V. P., Granskog, M. A., Dorn, W., Kayser, M., and Maturilli,  
534 M.: A comparison of the two Arctic atmospheric winter states observed during N-ICE2015 and SHEBA, *J. Geophys. Res.-*  
535 *Atmospheres*, 122, 5716-5737, doi: 10.1002/2016JD025475, 2017.

536 Graham, R. M., Itkin, P., Meyer, A., Sundfjord, A., Spreen, G., Smedsrud, L. H., Liston, G. E., Cheng, B., Cohen, L., Divine,  
537 D., Fer, I., Fransson, A., Gerland, S., Haapala, J., Hudson, S. R., Johansson, A. M., King, J., Merkouriadi, I., Peterson, A. K.,  
538 Provost, C., Randelhoff, A., Rinke, A., Rosel, A., Sennechael, N., Walden, V., Duarte, P., Assmy, P., Steen, H., and Granskog,  
539 M. A.: Winter storms accelerate the demise of sea ice in the Atlantic sector of the Arctic Ocean, *Sci. Rep.-Uk*, 9, Artn 9222,  
540 doi: 10.1038/S41598-019-45574-5, 2019.

541 Granskog, M. A., Fer, I., Rinke, A., and Steen, H.: Atmosphere-Ice-Ocean-Ecosystem Processes in a Thinner Arctic Sea Ice  
542 Regime: The Norwegian Young Sea ICE (N-ICE2015) Expedition, *J. Geophys. Res.-Oceans*, 123, 1586-1594, doi:  
543 10.1002/2017jc013328, 2018.

544 Hegseth, E. N.: Sub-Ice Algal Assemblages of the Barents Sea - Species Composition, Chemical-Composition, and Growth-  
545 Rates, *Polar. Biol.*, 12, 485-496, 1992.

546 Hudson, S. R., Cohen, L., Walden, V.: N-ICE2015 surface meteorology [Data set], Norwegian Polar Institute,  
547 <https://doi.org/10.21334/npolar.2015.056a61d1>, 2015.

548 Hudson, S. R., Cohen, L., Walden, V.: N-ICE2015 surface broadband radiation data [Data set], Norwegian Polar Institute,  
549 <https://doi.org/10.21334/npolar.2016.a89cb766>, 2016.

550 Hunke, E. C., Lipscomb, W. H., Turner, A. K., Jeffery, N., Elliot, S.: CICE: the Los Alamos Sea Ice Model. Documentation  
551 and User's Manual Version 5.1. Los Alamos National Laboratory, USA. LA-CC-06-012, 2015.

552 Ingram, R. G., Osler, J. C., and Legendre, L.: Influence of Internal Wave-Induced Vertical Mixing on Ice Algal Production in  
553 a Highly Stratified Sound, *Estuar. Coast. Shelf. S.*, 29, 435-446, doi: 10.1016/0272-7714(89)90078-4, 1989.

554 Jeffery, N., Hunke, E. C., and Elliott, S. M.: Modeling the transport of passive tracers in sea ice, *J. Geophys. Res.-Oceans*,  
555 116, Artn C07020, doi:10.1029/2010jc006527, 2011.

556 Jeffery, N., Elliott, S., Hunke, E. C., Lipscomb, W. H., Turner, A. K.: Biogeochemistry of CICE: The Los Alamos Sea Ice  
557 Model, Documentation and User's Manual. Zbgc\_colpkg modifications to Version 5, Los Alamos National Laboratory, Los  
558 Alamos, N. M., 2016.

559 Jin, M., Deal, C. J., Wang, J., Shin, K. H., Tanaka, N., Whitley, T. E., Lee, S. H., and Gradinger, R. R.: Controls of the  
560 landfast ice-ocean ecosystem offshore Barrow, Alaska, *Ann. Glaciol.*, 44, 9, 2006.

561 Jin, M., Deal, C., and Jia, W.: A coupled ice-ocean ecosystem model for I-D and 3-D applications in the Bering and Chukchi  
562 Seas, *Chinese Journal of Polar Science*, 19, 11, 2008.

563 Krause, J. W., Duarte, C. M., Marquez, I. A., Assmy, P., Fernandez-Mendez, M., Wiedmann, I., Wassmann, P., Kristiansen,  
564 S., and Agusti, S.: Biogenic silica production and diatom dynamics in the Svalbard region during spring, *Biogeosciences*, 15,  
565 6503-6517, doi: 10.5194/bg-15-6503-2018, 2018.

566 Lake, R. A., Lewis, E. L.: Salt rejection by sea ice during growth, *J. Geophys. Res.*, 75, 583-597, 1970.

567 Lannuzel, D., Tedesco, T., van Leeuwe, M., Campbell, K., Flores, H., Delille, B., Miller, L., Stefels, J., Assmy, P., Bowman,  
568 J., Brown, K., Castellani, G., Chierici, M., Crabeck, O., Damm, E., Else, B., Fransson, A., Fripiat, F., Geilfus, N. X., Jacques,  
569 C., Jones, E., Kaartokallio, H., Kotovitch, M., Meiners, K., Moreau, S., Nomura, D., Peeken, I., Rintala, J. M., Steiner, N.,  
570 Tison, J. L., Vancoppenolle, M., Van der Linden, F., Vichi, M. and Wongpan, P.: The future of Arctic sea-ice biogeochemistry  
571 and ice-associated ecosystems, *Nat. Clim. Change* 10(11), 983-992, doi: <https://doi.org/10.1038/s41558-020-00940-4>, 2020.

572 Lavoie, D., Denman, K., and Michel, C.: Modeling ice algal growth and decline in a seasonally ice-covered region of the  
573 Arctic (Resolute Passage, Canadian Archipelago), *J. Geophys. Res.-Oceans*, 110, Artn C11009, doi: 10.1029/2005jc002922,  
574 2005.

575 Leu, E., Mundy, C. J., Assmy, P., Campbell, K., Gabrielsen, T. M., Gosselin, M., Juul-Pedersen, T., and Gradinger, R.: Arctic  
576 spring awakening - Steering principles behind the phenology of vernal ice algal blooms, *Progr. Oceanogr.*, 139, 151-170, doi:  
577 10.1016/j.pocean.2015.07.012, 2015.

578 Lim, S. M., Moreau, S., Vancoppenolle, M., Deman, F., Roukaerts, A., Meiners, K. M., Janssens, J., and Lannuzel, D.: Field  
579 Observations and Physical-Biogeochemical Modeling Suggest Low Silicon Affinity for Antarctic Fast Ice Diatoms, *J Geophys*  
580 *Res-Oceans*, 124, 7837-7853, 10.1029/2018jc014458, 2019.

581 Mann, K. H., Lazier, J. R. N.: *Dynamics of Marine Ecosystems*, Third Edition, Blackwell Publishing Ltd., Carlton, Victoria  
582 3053, Australia, 503p., doi:10.1002/9781118687901, 2005.

583 McPhee, M.: *Air-ice-ocean interaction: Turbulent ocean boundary layer exchange processes*. Springer-Verlag, New York,  
584 216p., doi: 10.1007/978-0-387-78335-2, 2008.

585 McPhee, M. G., Morison, J. H., and Nilsen, F.: Revisiting heat and salt exchange at the ice-ocean interface: Ocean flux and  
586 modeling considerations, *J. Geophys. Res.-Oceans*, 113, Artn C06014, doi: 10.1029/2007jc004383, 2008.

587 Mortenson, E., Hayashida, H., Steiner, N., Monahan, A., Blais, M., Gale, M. A., Galindo, V., Gosselin, M., Hu, X. M., Lavoie,  
588 D., and Mundy, C. J.: A model-based analysis of physical and biological controls on ice algal and pelagic primary production  
589 in Resolute Passage, *Elem. Sci. Anth.*, 5, Artn 39, doi:10.1525/Elementa.229, 2017.

590 Nelson, D. M., and Treguer, P.: Role of Silicon as a Limiting Nutrient to Antarctic Diatoms - Evidence from Kinetic-Studies  
591 in the Ross Sea Ice-Edge Zone, *Mar. Ecol. Prog. Ser.*, 80, 255-264, doi: 10.3354/meps080255, 1992.

592 Niedrauer, T. M., and Martin, S.: Experimental-Study of Brine Drainage and Convection in Young Sea Ice, *J. Geophys. Res.-*  
593 *Oceans*, 84, 1176-1186, doi: 10.1029/JC084iC03p01176, 1979.

594 Notz, D., and Worster, M. G.: Desalination processes of sea ice revisited, *J Geophys Res-Oceans*, 114, Artn C05006, doi:  
595 10.1029/2008jc004885, 2009.

596 Olsen, L. M., Laney, S. R., Duarte, P., Kauko, H. M., Fernández-Méndez, M., Mundy, C. J., Rösel, A., Meyer, A., Itkin, P.,  
597 Cohen, L., Peeken, I., Tatarek, A., Róžańska, M., Wiktor, J., Taskjelle, T., Pavlov, A. K., Hudson, S. R., Granskog, M. A.,  
598 Hop, H., and Assmy, P.: The seeding of ice-algal blooms in Arctic pack ice: the multiyear ice seed repository hypothesis, *J*  
599 *Geophys Res-Biogeosciences*, 122(7), 1529-1548, doi: 10.1002/2016jg003668, 2017.

600 Olsen, L. M., Duarte, P., Peralta-Ferriz, C., Kauko, H. M., Johansson, M., Peeken, I., Róžańska-Pluta, M., Tatarek, A., Wiktor,  
601 J., Fernández-Méndez, M., Wagner, P. M., Pavlov, A. K., Hop, H., and Assmy, P.: A red tide in the pack ice of the Arctic  
602 Ocean, *Sci Rep*, 9, 9536, 10.1038/s41598-019-45935-0, 2019.

603 Peterson, A. K., Fer, I., Randelhoff, A., Meyer, A., Håvik, L., Smedsrud, L. H., Onarheim, L., Muilwijk, M., Sundfjord, A.,  
604 McPhee, M. G.: N-ICE2015 Ocean turbulent fluxes from under-ice turbulence cluster (TIC) [Data set], Norwegian Polar  
605 Institute, <https://doi.org/10.21334/npolar.2016.ab29f1e2>, 2016.

606 Reeburgh, W. S.: Fluxes Associated with Brine Motion in Growing Sea Ice, *Polar Biol.*, 3, 29-33, doi: 10.1007/Bf00265564,  
607 1984.

608 Rinke, A., Maturilli, M., Graham, R. M., Matthes, H., Handorf, D., Cohen, L., Hudson, S. R., and Moore, J. C.: Extreme  
609 cyclone events in the Arctic: Wintertime variability and trends, *Environ. Res. Letters*, 12, Artn 094006, doi:10.1088/1748-  
610 9326/Aa7def, 2017.

611 Smith, R. E. H., Cavaletto, J. F., Eadie, B. J., and Gardner, W. S.: Growth and Lipid-Composition of High Arctic Ice Algae  
612 during the Spring Bloom at Resolute, Northwest-Territories, Canada, *Mar. Ecol. Prog. Ser.*, 97, 19-29, doi:  
613 10.3354/meps097019, 1993.

614 Takeda, S.: Influence of iron availability on nutrient consumption ratio of diatoms in oceanic waters, *Nature*, 393, 774-777,  
615 doi: 10.1038/31674, 1998.

616 Tedesco, L., Vichi, M.: BFM-SI: a new implementation of the Biogeochemical Flux Model in sea ice. in: *CMCC Research*  
617 *Papers*, <http://www.cmcc.it/publications-meetings/publications/researchpapers/rp0081-ans-03-2010>,  
618 <http://hdl.handle.net/2122/5956>, 2010.

619 Tedesco, L., Vichi, M., and Scoccimarro, E.: Sea-ice algal phenology in a warmer Arctic, *Sci. Adv.*, 5, ARTN eaav4830, doi:  
620 10.1126/sciadv.aav4830, 2019.

621 Thomas, M., Vancoppenolle, M., France, J. L., Sturges, W. T., Bakker, D. C. E., Kaiser, J., and von Glasow, R.: Tracer  
622 Measurements in Growing Sea Ice Support Convective Gravity Drainage Parameterizations, *J Geophys Res-Oceans*, 125,  
623 ARTN e2019JC015791, doi: 10.1029/2019JC015791, 2020.

624 Turner, A. K., Hunke, E. C., and Bitz, C. M.: Two modes of sea-ice gravity drainage: A parameterization for large-scale  
625 modeling, *J. Geophys. Res.-Oceans*, 118, 2279-2294, doi: 10.1002/jgrc.20171, 2013.

626 Urrego-Blanco, J. R., Urban, N. M., Hunke, E. C., Turner, A. K., and Jeffery, N.: Uncertainty quantification and global  
627 sensitivity analysis of the Los Alamos sea ice model, *J. Geophys. Res.-Oceans*, 121, 2709-2732, doi: 10.1002/2015JC011558,  
628 2016.

629 Vancoppenolle, M., Bitz, C. M., and Fichefet, T.: Summer landfast sea ice desalination at Point Barrow, Alaska: Modeling  
630 and observations, *J. Geophys. Res.-Oceans*, 112, Artn C04022, doi: 10.1029/2006jc003493, 2007.

631 Vancoppenolle, M., Goosse, H., de Montety, A., Fichefet, T., Tremblay, B., and Tison, J. L.: Modeling brine and nutrient  
632 dynamics in Antarctic sea ice: The case of dissolved silica, *J Geophys Res-Oceans*, 115, Artn C02005, doi:  
633 10.1029/2009jc005369, 2010.

634 Vancoppenolle, M., Bopp, L., Madec, G., Dunne, J., Ilyina, T., Halloran, P. R., and Steiner, N.: Future Arctic Ocean primary  
635 productivity from CMIP5 simulations: Uncertain outcome, but consistent mechanisms, *Global Biogeochem Cy*, 27, 605-619,  
636 doi: 10.1002/gbc.20055, 2013.

637 van Leeuwe, M. A., Tedesco, L., Arrigo, K. R., Assmy, P., Campbell, K., Meiners, K. M., Rintala, J. M., Selz, V., Thomas,  
638 D. N. and Stefels, J.: Microalgal community structure and primary production in Arctic and Antarctic sea ice: A synthesis.  
639 *Elem. Sci. Anth.*, 6:4., doi: <https://doi.org/10.1525/elementa.267>, 2018.

640 Wakatsuchi, M., and Ono, N.: Measurements of Salinity and Volume of Brine Excluded from Growing Sea Ice, *J. Geophys.*  
641 *Res.-Oceans*, 88, 2943-2951, doi: 10.1029/JC088iC05p02943, 1983.

642 Webster, M. A., Rigor, I. G., Nghiem, S. V., Kurtz, N. T., Farrell, S. L., Perovich, D. K. and Sturm, M.: Interdecadal changes  
643 in snow depth on Arctic sea ice, *J. Geophys. Res.-Oceans* 119(8), 5395-5406, doi:10.1002/2014JC009985, 2014.

644 Wells, A. J., Wettlaufer, J. S., and Orszag, S. A.: Brine fluxes from growing sea ice, *Geophys Res Lett*, 38, Artn L04501, doi:  
645 10.1029/2010gl046288, 2011.  
646  
647  
648  
649  
650  
651